

Sphere Shaping with Dispersion-Aware Sequence Selection for Long-Haul Transmission Systems

Jingtian Liu⁽¹⁾, Élie Awwad⁽¹⁾, Hartmut Hafermann⁽²⁾, Yves Jaouën⁽¹⁾

Abstract—We introduce a nonlinear-tolerant design approach to Enumerative Sphere Shaping (ESS) for M -QAM signaling, utilizing sequence selection techniques based on a sign-independent metric: the Energy Dispersion Index, EDI (a scheme denoted E-ESS) and a novel sign-dependent metric: EDI of a dispersed sequence, D-EDI (a scheme denoted D-E-ESS). These approaches are designed to minimize rate loss and enhance transmission performance in nonlinear optical fiber transmission systems, catering to both short-distance and long-haul scenarios. Our simulation results reveal significant performance gains over conventional ESS, with improvements up to 0.4 bits/4D-symbol. These improvements were observed over a 205 km single-span standard single mode fiber link in WDM transmission, with five dual-polarization channels, each operating at a net rate of 400 Gbit/s. Furthermore, we demonstrate that D-E-ESS surpasses conventional ESS by 0.03 bits/4D-symbol in achievable information rate over a 30 span link with 80 km span in a single-wavelength 8 discrete multi-bands (DMB) transmission with an 880 Gbit/s net rate per channel, achieving similar performance to sequence selection based on a full split-step Fourier method (SSFM) simulation. We also demonstrate that D-EDI exhibits a more accurate negative correlation with the transmission performance compared to EDI. Notably, our proposed D-E-ESS scheme maintains robust performance improvements even when we consider reduced-complexity versions of it, consistently delivering throughput enhancements across various block lengths and selected sequence lengths.

Index Terms—Probabilistic shaping, sequence selection, fiber non-linearity, coherent transmission systems.

I. INTRODUCTION

Numerous studies have shown that achieving high throughput in optical fiber transmission systems is feasible through the utilization of techniques like Polarization Division Multiplexing (PDM), combined with M -ary Quadrature Amplitude Modulation (QAM) formats and Forward Error Correction (FEC) codes [1]–[3]. However, this increased efficiency often comes at the cost of reduced transmission distances due to effects such as OSNR limitation and Kerr-induced nonlinear distortions [4]. To approach the Shannon limit over an Additive White Gaussian Noise (AWGN) channel, the concept of constellation shaping has emerged as a promising strategy. Kschischang and Pasupathy's work demonstrated that the probability distribution that maximizes the achievable information rate over an AWGN channel, while maintaining a

fixed average energy constraint, corresponds to the Maxwell-Boltzmann (MB) distribution [5]–[7].

To effectively implement the MB distribution, various Distribution Matching (DM) techniques have been proposed for Probabilistic Constellation Shaping (PCS). Notable methods include enumerative sphere shaping (ESS) [8] and constant composition distribution matching (CCDM) [9]. CCDM [9] has emerged as a competitive technique for implementing PCS with rectangular or square M -QAM constellations by delivering near-optimal linear shaping gains when large amplitude blocks are considered [10]. However, in the context of mitigating Kerr-induced nonlinear interference (NLI) in optical fiber transmission, long block length DM may exhibit a higher susceptibility to performance degradation, as highlighted in previous analyses [11]–[13]. These works showed that short block length DM can effectively reduce NLI in optical fiber transmission. Yet, it is crucial to consider that, as the block length decreases, the rate loss increases. Hence, finding a high-performance nonlinear tolerant shaping scheme involves striking a trade-off between nonlinear gain and rate loss [14]. Besides, simulation results in [15], [16] showed that carrier phase recovery (CPR) in the DSP chain at the receiver side can exhibit comparable effectiveness to finite-length PCS in mitigating NLI.

To further enhance the nonlinear performance of PCS schemes, recent research efforts focused on introducing constraints in the trellis grid tree of ESS. For instance, in [17], the concept of kurtosis-limited ESS (K-ESS) was introduced as an extension of ESS. K-ESS not only has a maximum energy limit but also imposes a maximum kurtosis limit on the output sequence. This leads to a reduced average one-dimensional (1D) amplitude kurtosis, which in turn offers an additional nonlinear gain. This effect is underpinned by the EGN model [18], which forecasts a more significant nonlinear penalty associated with higher kurtosis levels. Subsequently, in [19], Band-Limited ESS (B-ESS) was introduced, which uses a specific subset of the trellis tree to limit 1D amplitude variance and kurtosis. B-ESS demonstrated superior performance compared to both K-ESS and conventional ESS. While both K-ESS and B-ESS implement sequences in four-dimensional (4D) space while applying energy limitations over each separate dimension, we proposed in a previous work [20] a band-limited version of ESS with energy limitations in 4D (two pairs of I and Q signals), achieving further throughput enhancement. However, for these three schemes, the rate loss was still significant.

Other design approaches of nonlinear tolerant signaling schemes consist in manipulating the input signal to the DM to generate multiple candidate sequences. Then, specific metrics

E-mail of corresponding author: jingtian.liu@telecom-paris.fr

⁽¹⁾ Communication and Electronics department, LTCI, Télécom Paris, Institut Polytechnique de Paris, 19 place Marguerite Perey, 91120 Palaiseau, France; ⁽²⁾ Optical Communication Technology Lab, Paris Research Center, Huawei Technologies, France.

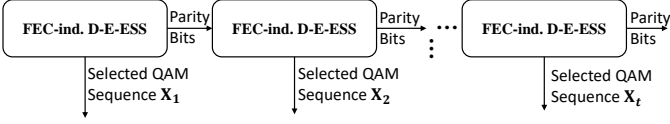


Fig. 1. Multi-block FEC-independent D-E-ESS sequence selection implementations. The parity bits from a current FEC-independent D-E-ESS block are allocated to a subset of the signs in the subsequent block.

are used to select “good” sequences, i.e., sequences generating low NLI. For example, the energy dispersion index (EDI), introduced in [21], is a metric that quantifies energy changes of the signal over a given temporal window. EDI showed a negative correlation with the effective Signal-to-Noise Ratio (SNR) of the CCDDM-based transmission; however, this negative correlation is observed in a single-polarization transmission scenario. As for ESS-based schemes, our study in [20] highlighted that the EDI, when calculated over 4D-energy levels, demonstrates a notable negative correlation for conventional ESS, B-ESS [19], and 4D-BL-ESS over 110 Gbaud, 400 km, 5 WDM transmission. However, this correlation appears to be inaccurate in the case of K-ESS [17]. In a different work [22], EDI was utilized for sequence selection in a scheme called List-Encoding CCDDM (L-CCDDM), achieving nonlinear gains with respect to conventional CCDDM. Yet, for long-haul transmissions, CCDDM is not the best distribution matcher, as similar nonlinear gains can be achieved through conventional ESS with shorter block lengths [14]. More recently, yet another approach, presented in [23], used EDI and a perturbation-model-based low-pass-filtered symbol-amplitude sequence (LSAS) metric [24] for sequence selection. These methods have substantially improved the nonlinear tolerance of ESS or CCDDM. However, it is essential to highlight that most significant gains in ESS schemes have been observed over short-distance single-span transmissions.

The concept of sequence selection (SS) was first introduced in [25] and has been further studied in [26]. This innovative signaling approach provided valuable insights into the computation of a lower bound of the optical fiber channel capacity. In particular, the analysis clearly showed that there is considerable room for improvement in optical fiber transmission, especially for long-haul links. A recent study [27] from the same authors emphasized the importance of enhancing performance through sequence selection using sign-dependent metrics in long-distance transmission scenarios. The authors demonstrated that sign-independent metrics such as EDI, windowed kurtosis, or LSAS do not yield significant throughput improvements over long-haul transmissions. They also showed that a sequence selection based on the computation of NLI through a numerical simulation (Split-Step Fourier Method or SSFM) of a noiseless single-channel propagation of sequences achieved throughput enhancements over long-distance transmissions even when an optimized CPR is applied. However, this selection method is not feasible in practice due to the high complexity of the SSFM.

In this paper, we introduce a novel sign-dependent metric, the EDI of dispersed sequences, named D-EDI, which accounts for the influence of chromatic dispersion throughout

the transmission process. Additionally, we show that D-EDI demonstrates a negative correlation with the effective SNR for high-rate multi-span transmission scenarios. Then, we propose two new sequence-selection ESS (SS-ESS) schemes designed for improving nonlinear tolerance: E-ESS, which uses sign-independent EDI sequence selection, and D-E-ESS¹, which employs sequence selection based on sign-dependent D-EDI. We thoroughly investigate and optimize the performance of these schemes in both single-span and multi-span transmission scenarios with optimized CPR. Our D-E-ESS scheme demonstrates superior performance compared to conventional ESS across various block lengths and complexity levels, in both single-channel and WDM transmission scenarios. Remarkably, it performs on par with the ideal SSFM-based sequence selection method, however with reduced complexity. The paper is structured as follows: in Section II, we recall some building blocks from recent literature that we reuse in our proposed scheme; then, in Section III, we define the new metric D-EDI and outline the architecture of the E-ESS and D-E-ESS transmitter schemes. Section IV focuses on the performance of a single-span transmission system and gives insights into the optimization of the proposed methods in this context. In Section V, we study the performance over multi-span single-channel and WDM transmission systems with CPR at the receiver side. Finally, Section VI summarizes key findings and conclusions drawn from our investigations.

II. INTRODUCTION TO MAPPING STRATEGY AND MULTI-BLOCK FEC-INDEPENDENT SEQUENCE SELECTION

A. Mapping Strategy

Distribution matching can be applied across different dimensions, including 1D, 2D, 4D, or even more. Fig. 3 in [28] provides a visual representation of the mapping strategies employed by ESS schemes up to four dimensions. In the case of 1D mapping, 4D symbols are shaped using four independent amplitude sequences, essentially employing one ESS per dimension. In 2D mapping, each polarization, namely X and Y, utilizes a distinct ESS-shaped amplitude sequence. In contrast, 4D mapping employs a single-shaped sequence for a dual-polarization symbol sequence. For example, assuming the amplitude sequence is $[a_1, a_2, \dots, a_8]$, the dual-polarization symbol sequence over two time slots employing 4D mapping will be:

$$\begin{bmatrix} S_{Pol.X,T_1} & S_{Pol.X,T_2} \\ S_{Pol.Y,T_1} & S_{Pol.Y,T_2} \end{bmatrix} = \begin{bmatrix} \pm a_1 \pm j a_2 & \pm a_5 \pm j a_6 \\ \pm a_3 \pm j a_4 & \pm a_7 \pm j a_8 \end{bmatrix} \quad (1)$$

This last approach offers the advantage of reducing the likelihood of having equal amplitudes at the same time slot, resulting in less frequent occurrences of high peak power values and leading to lower levels of non-linear distortions. This advantage has been demonstrated in various studies [11], [17], [28]. Hence, in our work, we use 4D mapping of the amplitudes at the output of the distribution matcher.

¹For an ESS system employing sequence selection based on either EDI or D-EDI and comprising n cascaded DMs, where each DM includes ν flipping bits, we name the scheme $E-ESS_n^\nu$ for the EDI-based approach, and $D-E-ESS_n^\nu$ for the D-EDI-based approach. The schemes will be detailed in section III.

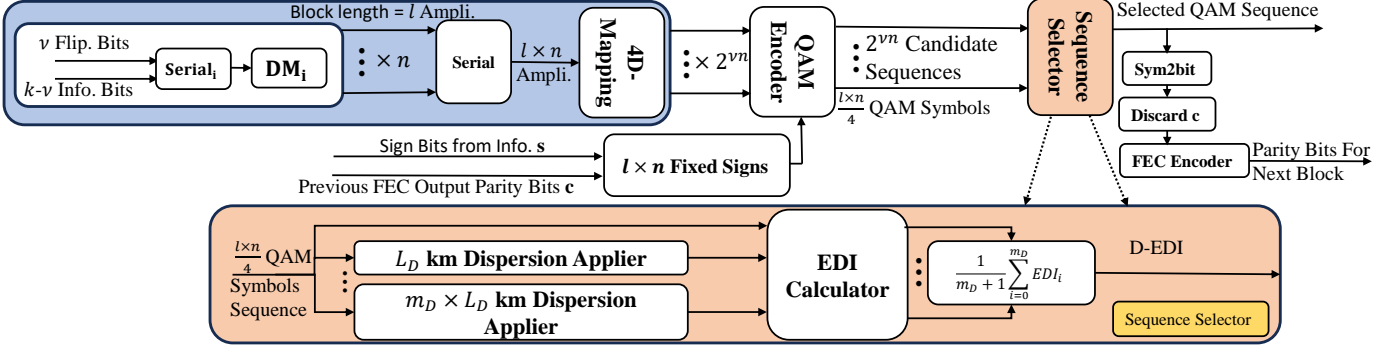


Fig. 2. Block diagram of FEC independent D-E-ESS in the PAS transmitter, EDI of dispersed sequences (D-EDI) is determined by averaging the calculated EDI at multiple locations along an ideal dispersive fiber. The dispersion is applied at 1 sample per symbol. EDI is a special case of D-EDI where $m_D = 0$. The sign bits are fixed through a multi-block FEC-independent sequence selection process as shown in Fig. 1.

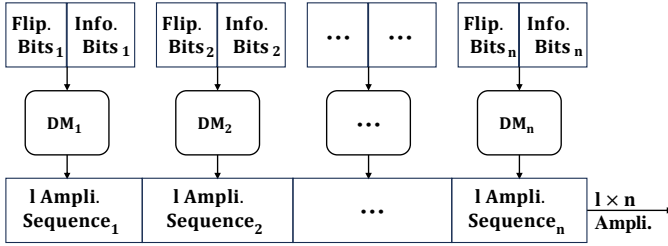


Fig. 3. Structure of cascaded distribution matchers (DMs). The output amplitude sequences of n DMs are concatenated to form a longer sequence.

B. Multi-Block FEC-Independent Sequence Selection

The goal of the multi-block FEC-independent SS scheme is to reduce the complexity by moving the FEC from before to after the sequence selection. The implementation of multi-block FEC-independent sequence selection was proposed in [27]. As shown in Fig. 1, the parity bits of each FEC-independent D-E-ESS block (a block that will be presented in Fig. 2 of the next section), are assigned to a portion of the signs in the subsequent block. In the process of selecting a specific sequence, these signs are predetermined by the parity bits from the preceding block. These predetermined signs are required for the calculation of a sign-dependent metric. It is important to note that, once the candidate sequences have been generated, their bits become fixed and unalterable. Consequently, if the FEC encoding is applied after the sequence selection (SS) process, it becomes necessary to shift the parity bits to the subsequent block.

III. E-ESS AND D-E-ESS DESIGN

The fundamental concept behind E-ESS draws inspiration from the list-CCDM [22]. Our approach allows for the use of various distribution matchers. In this study, we specifically focus on ESS. In Fig. 2, we plot the encoding process where input bits are fed into a 1D ESS distribution matcher (DM) with block length l that generates l amplitudes. The input bit stream is composed of two parts: $k - \nu$ information bits and ν prefix flipping bits. Altering these ν prefix flipping bits can cause pronounced changes in the sequences' indices during the ESS encoding process. Such changes are reflected

as considerable alterations in the amplitudes across the block. Conveniently, these flipping bits are discarded after the decoding process at the receiver side.

We may cascade the outputs of n 1D-DMs sequentially to generate a longer sequence, which can then undergo a selection process as shown in Fig. 3. This resulting sequence will have a length of $l \times n$. Cascading DMs have two advantages: it permits obtaining more candidate sequences while maintaining the same rate loss, and at the same time, we maintain the use of short-block-length DMs that show a clear advantage against long-block-length DM with respect to non-linear effects. For an E-ESS (or a D-E-ESS) with n cascaded DMs, where each DM includes ν flipping bits, we can generate $2^{\nu n}$ different candidate sequences. Subsequently, the $l \times n$ amplitudes are mapped to $(l \times n)/4$ 4D-QAM symbols. E-ESS employs EDI as a metric for sequence selection, which is a sign-independent metric defined in Eq. (2) below taken from [21]. $\mathbf{X} = [\dots \mathbf{X}_{i-1}, \mathbf{X}_i, \mathbf{X}_{i+1}, \dots]$ represents a series of 4D complex symbols, and w is the EDI averaging window length, expressed as a number of symbols, and it is directly linked to the two-sided channel memory, denoted $2M$ and given by $2M = 2 \lfloor \pi |\beta_2| B R_s L \rfloor$. In this formula, β_2 stands for the group velocity dispersion, B is the channel spacing, R_s is the symbol rate, and L represents the transmission distance. $\lfloor \cdot \rfloor$ denotes the rounding operation to the nearest integer. As observed in previous works such as in [21] (specifically in their Fig. 9), the optimal window length w , defined as the length where the correlation between EDI and SNR is maximized, is typically less than $2M$. G_i^w is the sum of the energies of $w + 1$ symbols centered on the symbol \mathbf{X}_i , as described by Eq. (3). The EDI, denoted as Ψ , is calculated as the ratio of the variance of the energy within the window (Eq. (4)) to the mean energy within the same window (Eq. (5)). This calculation is averaged across $i = \{\frac{w}{2} + 1, \dots, L_s - \frac{w}{2}\}$, where L_s is the sequence length. $L_s = (l \times n)/4$ in scenarios where 4D mapping is applied in conjunction with cascaded DMs.

$$\Psi \triangleq \frac{\overline{\text{Var}}[G^w]}{\overline{E}[G^w]} \quad (2)$$

$$G_i^w \triangleq \sum_{j=i-w/2}^{i+w/2} |X_j|^2 \quad (3)$$

$$\overline{Var}[G^w] \triangleq \frac{1}{L_s - w} \sum_{i=\frac{w}{2}+1}^{L_s - \frac{w}{2}} Var[G_i^w] \quad (4)$$

$$\overline{E}[G^w] \triangleq \frac{1}{L_s - w} \sum_{i=\frac{w}{2}+1}^{L_s - \frac{w}{2}} E[G_i^w] \quad (5)$$

Consequently, the assigned signs to the generated amplitudes are not necessary for the evaluation of the metric. After 4D-mapping [28], the sequence selector (EDI calculator) is presented with $2^{\nu n}$ candidate sequences, each with a length of $(l \times n)/4$ 4D-QAM symbols. The sequence selector then identifies and transmits the sequence with the lowest 4D-energy EDI.

To further boost the performance of sequence selection over long-haul links, we introduce sequence selection ESS based on D-EDI. Within the sequence selector, the EDI of dispersed sequences, abbreviated as D-EDI and denoted as Ψ_D in Eq. (6), is calculated by averaging the EDI values obtained at multiple points along a linear dispersive fiber without attenuation, as illustrated in Fig. 2. Here, \mathbf{X}_m designates the symbol sequence that has propagated over $m \times L_D$ kilometers of a linear dispersive fiber without attenuation. $\mathfrak{D}_{D,x}$ in Eq. (7) represents the chromatic dispersion operator of a fiber with a dispersion coefficient D in ps/nm/km and length x km.

$$\Psi_D \triangleq \frac{1}{m_D + 1} \sum_{m=0}^{m_D} \Psi[\mathbf{X}_m]. \quad (6)$$

$$\mathbf{X}_m \triangleq \mathfrak{D}_{D,m \times L_D}[\mathbf{X}]. \quad (7)$$

Dispersion is digitally applied over the symbol sequence sampled at one sample per symbol. D-EDI is a metric that requires knowledge of sign bits to compute the form of a dispersed sequence. EDI is the special case of D-EDI where $m_D = 0$. The sign bits can be fixed through a multi-block FEC-independent sequence selection process as illustrated in Sec. II-B. In this scenario, the sign bits are chosen in two parts: a part from the information stream of the current D-E-ESS block, denoted \mathbf{s} , and a part from the FEC output parity bits of the previous D-E-ESS block, denoted \mathbf{c} . Once the QAM sequence is selected, it is demapped into a bit sequence and sent into a FEC encoder after discarding the parity bits from the previous D-E-ESS block, \mathbf{c} , to generate parity bits for the next D-E-ESS block.

For a single-span link, one may apply D-EDI by cutting the span into multiple sections and adding up EDIs computed over the first sections given that nonlinear distortions are more important at the beginning of each span, where the signal power is still high. In what follows, to keep the computational complexity low for a single-span link, we add up two EDIs, the one computed over the sequences at the transmitter side and the one computed after propagation over the effective length of the fiber span $L_{D(\text{single span})} = L_{eff} = \frac{1 - \exp(-\alpha L)}{\alpha}$ [29] where α is the fiber attenuation in km^{-1} and L is the length of the fiber span in km. For a multi-span link of m spans of length L km each, we may add up the EDIs computed over sequences at the beginning of each span. For the sequence at the

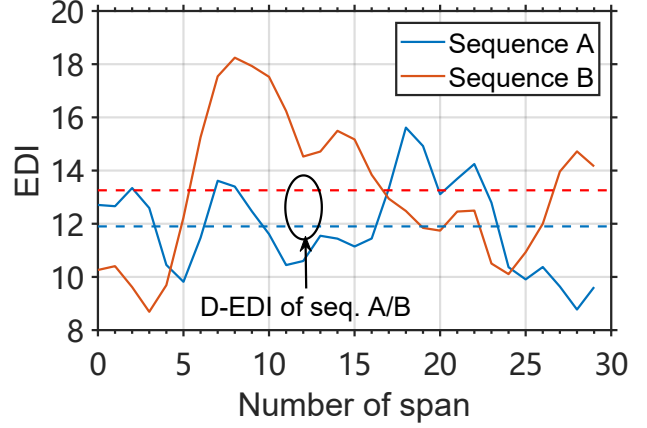


Fig. 4. Simulation in single channel, 8 DMB subcarriers, 110 GBaud transmission over 30×80 km SSMF link, with a net rate of 880 Gbit/s. Sequences A and B are two randomly generated sequences over the 4th subcarrier, each consisting of 108 4D 64-QAM symbols. Solid lines represent the evolution of EDI at the beginning of each span, dashed lines represent D-EDI computed as an averaged EDI over all spans. D-EDI gives a more accurate estimation of NLI generated by each sequence after transmission.

beginning of the last span, we apply dispersion corresponding to $m_D L_D = (m - 1)L$ km.

Both E-ESS and D-E-ESS increase the rate loss in each dimension by $\frac{\nu}{l}$ as in [23], which is an extra rate loss term that accounts for the effect of the flipping bits. The total rate loss R_{loss} in each dimension is:

$$R_{loss} = H(P_a) - \frac{k - \nu}{l}. \quad (8)$$

where $H(P_a)$ is the entropy linked to the distribution P_a and P_a is the marginal distribution of the amplitudes of the PAM symbols. As the value of ν increases, the number of candidate sequences also increases, resulting in higher nonlinear shaping gain. However, this comes at the cost of increased rate loss. As a result, an efficient sequence selection mechanism should strike a balance between linear and nonlinear shaping gains. On another note, the utilization of prefix flipping bits eliminates the need for look-up tables (LUTs) and XOR operations proposed in the bit scrambling method in [27], hence simplifying the implementation complexity and avoiding the additional memory requirements of LUTs. Finally, D-EDI computation has clearly a much lower complexity compared to the SSFM-based average NLI metric in [27].

In Fig. 4, we illustrate the evolution of the EDI metric at the beginning of each span when transmitting two different random sequences over a 30×80 km link with a single channel, 8 DMB subcarriers, 110 GBaud transmission, and a net rate of 880 Gbit/s. Each of these sequences comprises 108 random 4D 64-QAM symbols over the 4th subcarrier. EDI is calculated at the beginning of each span and both EDI and D-EDI employ a window length of 2 symbols ($w = 2$), that is 1 symbol before and 1 symbol after the current symbol. Before transmission, sequence B exhibits a lower EDI compared to sequence A. This implies that sequence B will generate less NLI over the first span than sequence A. However, as the sequences propagate through the dispersive fiber, their characteristics

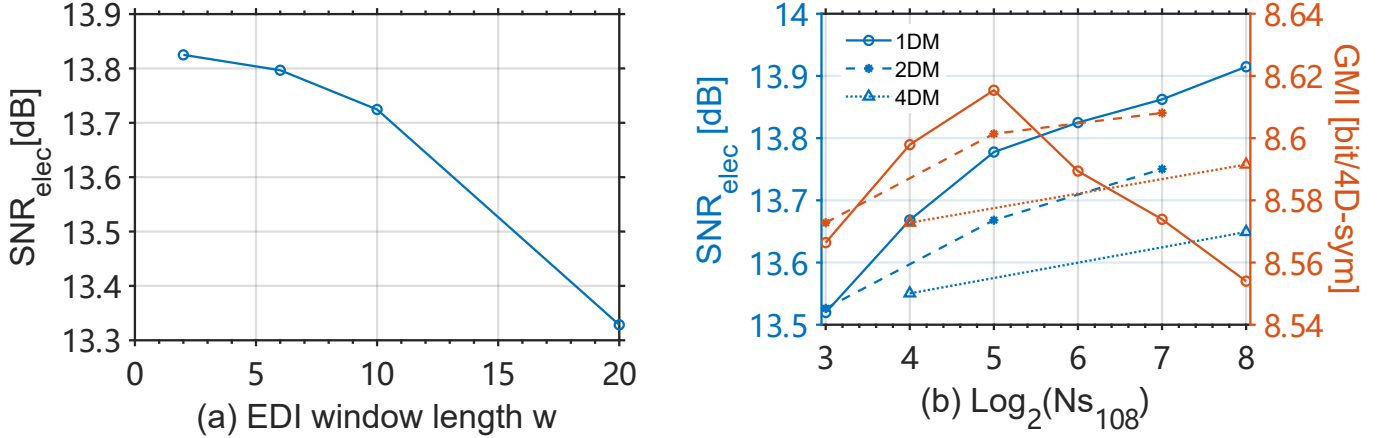


Fig. 5. Simulation of 50 GBaud E-ESS transmission over 205 km single span SSMF link, 5 WDM channels, 55 GHz channel spacing, net rate per channel 400 Gbit/s. (a): Electrical SNR versus the EDI window length w used in the sequence selector to evaluate the EDI of sequences. $\nu = 3$ flipping bits and a single 1D-DM ($n = 1$) is used. The power per channel is 9 dBm. (b): Electrical SNR and GMI at 9 dBm versus $\log_2(N_{S108})$ when cascading 1, 2 or 4 DMs, where N_{S108} is the number of required sequence selections to generate 108 4D-symbols. $E\text{-ESS}_1^3$ exhibits the highest performance in terms of GMI.

change continuously due to the influence of dispersion. After only 4 spans, the EDI of sequence B surpasses that of sequence A. Ultimately, when the D-EDI is computed by averaging EDI over all spans, sequence A yields a smaller D-EDI even though it had a larger initial EDI. This suggests that sequence A maintains a higher average nonlinear shaping gain throughout the entire transmission. This outcome emphasizes the importance of considering sign-dependent metrics, such as D-EDI, when assessing the nonlinear shaping gain performance of sequences. Sign-independent metrics may not provide a complete picture of NLI manifestation, as the influence of dispersion can cause initially favorable sequences to show deteriorated performance after a certain propagation distance, while initially unfavorable sequences may show an improved performance. Hence, D-EDI allows for a more accurate estimation of NLI generated by each sequence throughout a transmission.

IV. PERFORMANCE ASSESSMENT: SINGLE-SPAN TRANSMISSION

We study the performance of E-ESS and D-E-ESS in two scenarios: first, a single-span transmission scenario similar to the one in [17], [19], and second, a multi-span long-haul transmission scenario using digital-multi-band (DMB) format. Through the two studies, we observe the effects of non-linear distortions over various transmission distances. It is important to remind that these distortions are dominant at higher power levels. Therefore, in a single-span transmission, they primarily occur over the first kilometers of the span. In contrast, in a multi-span scenario with discrete optical amplification, NLI distortions are added at the start of each span.

We conduct a performance evaluation of the E-ESS and D-E-ESS systems using PDM 64-QAM modulation with a block length of $l = 108$ to align with the conditions described in [17], [19]. Our transmitted signal comprised 5 Wavelength-Division Multiplexing (WDM) channels, each operating at 50 GBaud, resulting in a raw data rate of 600 Gbit/s per

channel. For all the tested ESS schemes, we employed a Low-Density Parity-Check (LDPC) code with a length of 64800 bits, following the DVB-S2 standard, and a code rate of $r_c = 5/6$. Consequently, the achieved net bit rate amounted to 8 bits per 4D symbol, resulting in a net bit rate of 400 Gbit/s per channel. The channel spacing is set to 55 GHz, and we apply root-raised cosine (RRC) pulse shaping with a roll-off factor of 0.1 to each channel. Standard single-mode fiber (SSMF) is simulated with an attenuation coefficient $\alpha = 0.2$ dB/km, chromatic dispersion coefficient $D = 17$ ps/nm/km, polarization mode dispersion (PMD) of 0.04 ps/ $\sqrt{\text{km}}$, and a nonlinear parameter $\gamma = 1.3$ (W · km) $^{-1}$ at $\lambda = 1550$ nm. Our simulated channel consists in a single-span transmission over a distance of 205 km, to perform a consistent comparison with [17], [19] in which the Kurtosis-limited (K-ESS) and band-limited (B-ESS) sphere shaping were introduced. We do not add any laser phase noise in the simulation. Following propagation, the central channel underwent several signal processing steps, including optical filtering, matched filtering, chromatic dispersion compensation, and genie-aided multiple-input-multiple-output (MIMO) channel equalization. Subsequently, we applied a fully-data-aided phase filter with a window averaging over 64 symbols to compensate for phase rotation induced by cross-phase modulation (XPM) as carrier phase recovery (CPR), as elaborated in [30]. Finally, we measured the electric SNR denoted SNR_{elec} from the equalized constellations and computed the generalized mutual information (GMI) using Eq. (10) from [31].

First, we focus on the E-ESS scheme. In Fig. 5 (a), we plot the SNR_{elec} for various EDI window lengths w used by the sequence selector. For this test, we used a single 1D-DM ($n = 1$) and $\nu = 3$ flipping bits and denote the scheme $E\text{-ESS}_1^3$ (or in general $E\text{-ESS}_n^\nu$). This setup allows us to select the most suitable sequence from eight possible candidates ($2^3 = 8$). We calculate SNR_{elec} using equalized symbols after transmitting over a single span with a channel power of 9 dBm, which is near the optimal power level.

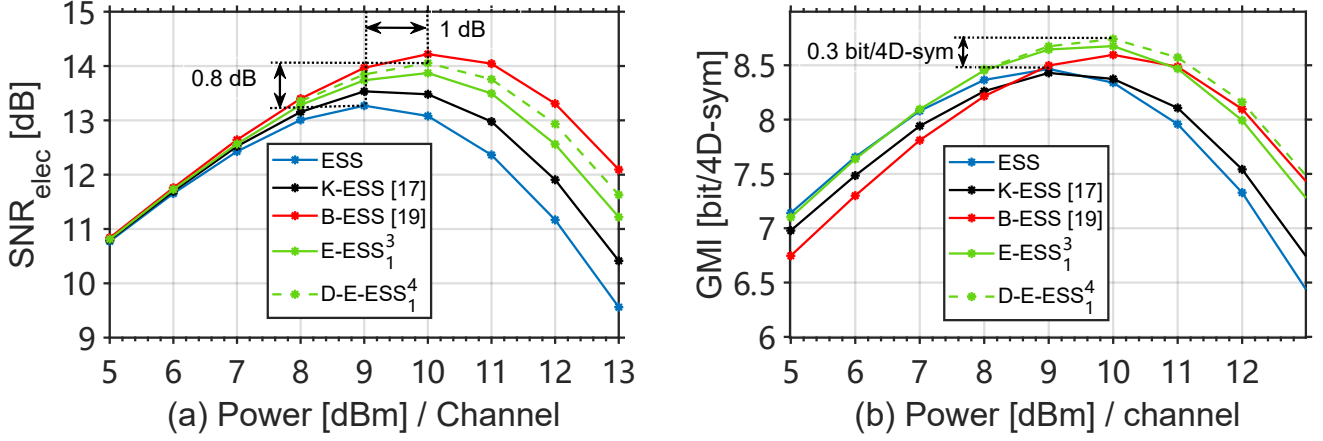


Fig. 6. Simulation of conventional ESS, K-ESS, B-ESS, $E-ESS_1^3$, and $D-E-ESS_1^4$ (best-performing scheme) with D-EDI computed after applying a single 21 km dispersion filter. Same system configuration as for Fig. 5. Left: Electrical SNR versus power per channel. Right: GMI versus power per channel. Both $E-ESS_1^3$ and $D-E-ESS_1^4$ demonstrate superior performance when compared to state-of-the-art schemes.

Our findings show that as w increases, the SNR_{elec} gradually declines. We find that a window length $w = 2$ yields the best performance, and is much lower than the channel memory ($2M = 76$ when considering the total length of the span). Therefore, we proceed with $w = 2$ in subsequent single-span simulations. In Fig. 5 (b), we analyze the performance of E-ESS by varying the number of sequentially cascaded DMs n , where each DM has ν flipping bits. As a complexity metric, we designate the number of tested candidate sequences per 108 4D-symbols. We choose 4 DMs as 4 is the least common multiple between the three studied values of $n = \{1, 2, 4\}$. Moreover, having a block length $l = 108$ per DM, 4 DMs will generate 108 4D symbols. We denote the number of tested sequences as $N_{S_{108}}$ which is given by:

$$N_{S_{108}} = \frac{4}{n} 2^{\nu n} \quad (9)$$

A single DM with a block length $l = 108$ produces 27 4D-symbols after 4D-mapping. Consequently, when cascading $n = 1, 2$, or 4 DMs, the candidate sequence lengths will be 27, 54, and 108 respectively. To achieve a total sequence of 108 4D symbols, the E-ESS transmitter needs to be called $\frac{4}{n}$ times, resulting in 4, 2, and 1 calls for $n = 1, 2$, and 4 cascaded DMs respectively. We see from Fig. 5 (b) that, as $N_{S_{108}}$ increases, SNR_{elec} also increases for $n = \{1, 2, 4\}$. However, as the number of flipping bits increases, the rate loss likewise increases. The maximum GMI is hence attained when achieving a trade-off between rate loss and nonlinear gain. Specifically, the largest GMI is achieved with a single 1D-DM at $\log_2(N_{S_{108}}) = 5$ (32 candidate sequences), corresponding to the $E-ESS_1^3$ configuration.

Next, we also evaluated the performance of the D-E-ESS scheme over the same link by computing D-EDI as the sum of the EDI of the sequence at the transmitter output and its EDI after propagating over a linear dispersive fiber without attenuation of length L_{eff} over which nonlinear effects remain significant. $n = 1$ and $\nu = 4$ ($D-E-ESS_1^4$) yield the best GMI gains through a similar optimization as the one shown in Fig. 5(b) for E-ESS. In Fig. 6 (a), we show SNR_{elec} versus the

launch power per channel for five different ESS schemes. The D-E-ESS, E-ESS, band-limited ESS (B-ESS), and kurtosis-limited ESS (K-ESS) exhibit SNR gains of approximately 0.8 dB, 0.6 dB, 1 dB, and 0.3 dB respectively, compared to the conventional ESS at a power level of 10 dBm. Additionally, they demonstrate up to 1 dB improvement in the optimal launch power. In Fig. 6 (b), we present the results in terms of GMI per 4D symbol. Notably, the D-E-ESS scheme yields the highest GMI. Specifically, at a power level of 10 dBm, it achieves a GMI increase of 0.15 bit/4D compared to B-ESS and a 0.3 bit/4D improvement compared to conventional ESS. The E-ESS scheme also delivers a GMI gain of 0.1 bit/4D (respectively 0.2 bit/4D) in comparison to B-ESS (respectively conventional ESS). It is important to mention that both EDI and D-EDI based shaping approaches exhibit nearly the same linear performance as unconstrained ESS due to their small rate loss. E-ESS and D-E-ESS exhibit similar performance largely because the initial shape of the waveform at the start of the link plays a crucial role in the generation of NLI for single span links. However, a slight performance improvement is achievable by selecting sequences that also exhibit low EDI after the effective length, L_{eff} . In terms of rate loss, D-E-ESS demonstrates superiority over B-ESS and K-ESS, with a rate loss of 0.26 bit/4D compared to 0.5 bit/4D and 0.27 bit/4D respectively. The rate losses are not discernible in Fig. 6 (b) between 5 dBm and the optimal power level because non-linear gains are already occurring within these power ranges. D-E-ESS also outperforms E-ESS in the nonlinear regime. Overall, it outperforms B-ESS in both linear and nonlinear regimes. Finally, we remind that D-E-ESS requires a slightly higher complexity compared to E-ESS since it necessitates knowledge of sign bits and computation of dispersed sequences at the transmitter side.

V. PERFORMANCE ASSESSMENT: MULTI-SPAN TRANSMISSION

We now evaluate the potential advantages of our schemes when applied to higher baud rate long-haul links employ-

ing digital-multi-band (DMB) signals known for their superior resistance to Kerr effects compared to single-carrier schemes [32], [33]. The baud rate in this scenario is set at 110 Gbaud, utilizing 8 subcarriers in a single-wavelength configuration. The transmission channel is 30×80 km standard single-mode fiber (SSMF) spans with EDFA amplification. The achieved net data rate per channel is 880 Gbit/s. The digital signal processing (DSP) blocks employed in this scenario are consistent with those detailed in the preceding section.

A. Optimization and Transmission Performance

In Fig. 7, we evaluate the performance of our D-E-ESS scheme for different cascaded DMs and different number of flipping bits. In long-distance links, accumulated chromatic dispersion becomes apparent as its induced inter-symbol interference involves hundreds of symbols. For these links, it becomes more important to cascade multiple 1D-DMs to generate extended candidate sequences over which we will compute D-EDI. By doing so, we account for the impact of the accumulated channel memory on the waveform, thus making a better selection process. In addition, for the same complexity level as a single DM, this approach helps in reducing rate loss. As we did in the previous section, the complexity of the scheme is evaluated as $N_{S_{108}}$, the number of tested candidate sequences for the generation of 108 4D-symbols. We calculate D-EDI by summing up EDI values of the sequences at the input of each of the 30 spans constituting the 30×80 km link ($w = 2$ corresponding to the memory of a 13.75 Gbaud transmission over a single 80 km span). We observe that, as $N_{S_{108}}$ increases, SNR_{elec} also increases. However, as the number of flipping bits per DM increases, the rate loss increases too. In the scenario of long-haul transmissions, the SNR gain is less significant compared to single-span transmissions. Consequently, the rate loss has a greater impact on the final performance. The trade-off between rate loss and nonlinear gain shows that the largest GMI occurs in the configuration where $n = 4$ 1D-DMs are arranged in series, and each 4D-DM has $\nu = 1$ flipping bit, denoted $D-E-ESS_4^1$, and corresponding to $\log_2(N_{S_{108}}) = 4$ (i.e. 16 candidate sequences). The GMI curve for 1DM exhibits a significantly steeper slope compared to the one for 4DM, as the rate loss increases at a slower pace in the case of cascading 4 DMs.

Next, in Fig. 8, we compare the performance of four single-wavelength transmission schemes: conventional ESS over a single carrier (SC) serving as a baseline, conventional ESS over DMB using 8 subcarriers (8DMB), $D-E-ESS_4^1$ (optimal case) schemes and $E-ESS_4^1$, both in 8DMB mode. The $D-E-ESS_4^1$ shows a 0.2 dB increase in SNR_{elec} and 0.03 bit/4D-symbol gain in GMI at a power of 4.5 dBm compared to conventional ESS with 8DMB and it shows a 0.66 dB increase in SNR_{elec} and 0.16 bit/4D in GMI at the optimal power compared to conventional ESS over a single carrier. We can also see that, even though the $E-ESS_4^1$ has a slight SNR gain, it does not counterbalance the rate loss, and eventually there is no gain in GMI with respect to conventional ESS. On the other hand, the sign-dependent-based D-E-ESS scheme maintains the GMI advantage in both

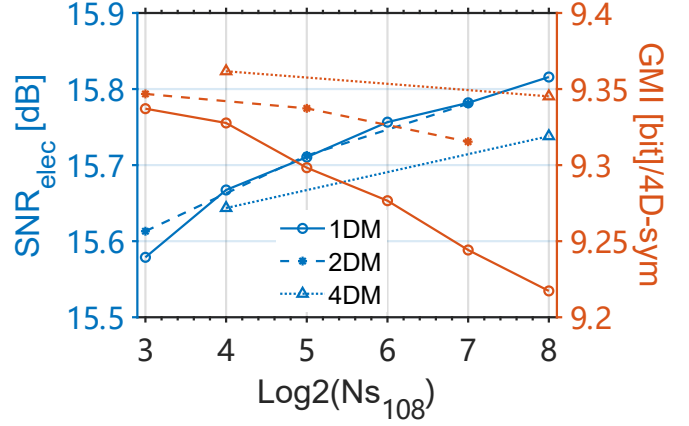


Fig. 7. Simulation of D-E-ESS with D-EDI computed after applying dispersion successively over 30×80 km, single channel, 8 DMB subcarriers, 110 Gbaud transmission, net rate per channel 880 Gbit/s. Electrical SNR and GMI versus $\log_2(N_{S_{108}})$ at the optimal power (4.5 dBm), where $N_{S_{108}}$ is the number of tested sequences per 108 4D-symbols. $D-E-ESS_4^1$ exhibits the highest performance in terms of GMI.

short-distance and long-haul distance transmissions. Additionally, we conducted simulations involving sequence selection based on the computation of the actual NLI produced by each sequence using the Split-step Fourier method (SSFM selection) to approximate an upper bound for the performance of a sequence selection scheme. We kept the transmitter structure as 4 concatenated DMs, each equipped with 1 flipping bit. This approach is similar to the one outlined in [27]. Each candidate sequence was transmitted over a 30×80 km standard single mode fiber, single-wavelength, single-carrier system operating at 13.75 Gbaud, without the addition of ASE noise. After transmission, we compare the NLI power of candidate sequences and select the sequence that generates the lowest NLI. This process allows us to obtain the optimal performance of sequence selection with 4 serial DMs, and 1 flipping bit when only considering self-phase modulation effects. From Fig. 8, we observe that SSFM-ESS and D-E-ESS exhibit almost identical performance. This observation indicates that within the analyzed system, selecting sequences based on D-EDI can be a viable alternative to the more complex SSFM approach. In other words, the variations of the waveform shaped by dispersion effects primarily dictates nonlinear distortions in high-power regions. Nonlinearity, in this context, acts as a small perturbation. Consequently, we can feasibly substitute SSFM with the dispersion-aware metric, D-EDI, for sequence selection.

B. Complexity Reduction and Interpretation of the Results

In the above study, we aimed to improve sequence selection by calculating the EDI at the beginning of each span along the entire transmission link. This resulted in obtaining 30 different EDI values, which were then averaged to derive the final D-EDI. Now, we delve into the impact of the computational complexity of D-EDI on the achieved performance. To reduce the computational load of D-EDI, we explore two methods. First, we consider calculating D-EDI for only the first $m_D =$

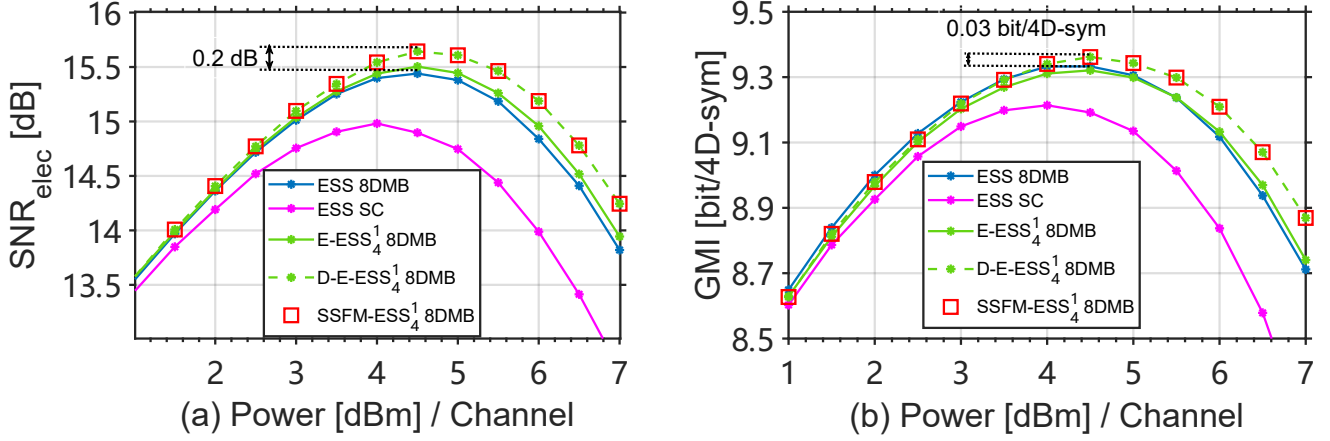


Fig. 8. Simulation of conventional ESS, $E-ESS_4^1$, $D-E-ESS_4^1$ and $SSFM-ESS_4^1$ with 30×80 km dispersion applier over 1 channel 8 DMB subcarriers, and conventional ESS with 1 channel 1 carrier, in 110 GBaud over 30×80 km SSFM link, net rate per channel 880 Gbit/s. (a): Electrical SNR versus Power per channel in the non-linear channel. (b): GMI versus Power per channel. $D-E-ESS_4^1$ exhibits the same performance as that of an ideal SSFM-based sequence selection.

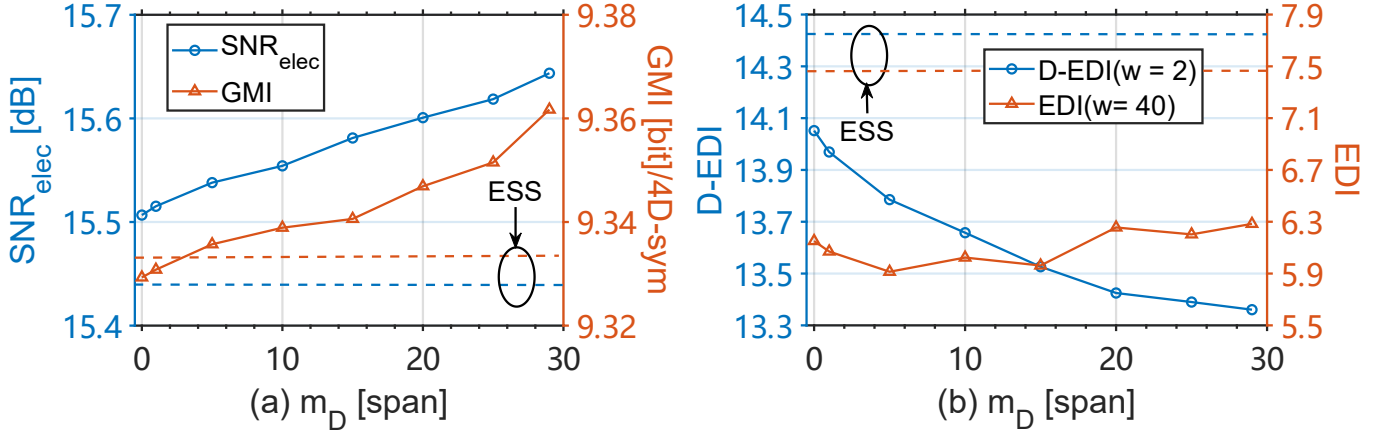


Fig. 9. Performance analysis of $D-E-ESS_4^1$ (a): Electrical SNR and GMI versus m_D at optimal power (4.5 dBm) where m_D is the maximum number of spans used by the dispersion applier during sequence selection. Gains are maintained even when we reduce the complexity by computing D-EDI over fewer spans. (b): D-EDI and EDI versus m_D . We add the values for conventional ESS by horizontal dashed lines. Same system configuration as in Fig. 7. D-EDI demonstrates a negative correlation with SNR_{elec} .

$\{1, \dots, 29\}$ spans instead of the entire transmission line. It is worth reminding that, when $m_D = 0$, D-EDI simplifies to original EDI. Second, we consider calculating D-EDI by summing up EDIs after the signal propagates through intervals of $N_D > 1$ spans instead of computing it at the beginning of each span ($N_D = 1$).

In Fig. 9, we explore the first method. In Fig. 9 (a), we present the performance results in terms of SNR_{elec} and GMI. We include the values for conventional ESS as horizontal dashed lines for comparison. SNR exhibits a steady growth as m_D increases. The peak value is achieved when $m_D = 29$, implying that D-EDI calculations across the entire link yield the maximum benefit. After only three spans, the nonlinear gain brought by D-EDI-based sequence selection overcomes the penalty in increased rate loss, resulting in a higher GMI than the one obtained with conventional ESS. These observations underscore the fact that in dispersion unmanaged transmission systems, nonlinear penalties are equally distributed

and independent across homogeneous spans as predicted by the GN [34] and EGN models [18]. Hence, to get the most out of sequence selection, it is crucial to calculate D-EDI for the entire link. Thereafter, in Fig. 9 (b), we illustrate the EDI and D-EDI values evaluated for the selected candidate sequences for different m_D values. EDI is evaluated over 40 symbols ($w = 40$), which is an empirical value lower than the total channel memory $2M = 68$ (corresponding to the channel memory of a 13.75 GBaud transmission over the entire link (30×80 km)) as explained in Sec. III; whereas D-EDI is assessed by averaging EDIs computed with a memory of 2 symbols ($w = 2$), corresponding to the memory of a 13.75 GBaud transmission over a single 80 km span. This D-EDI used for performance evaluation of the selected sequences is calculated along the entire link. Notably, As m_D increases, D-EDI continues to decrease and hence exhibits a negative correlation with SNR_{elec} , while EDI struggles to do so, showing that D-EDI is a better estimator of the performance

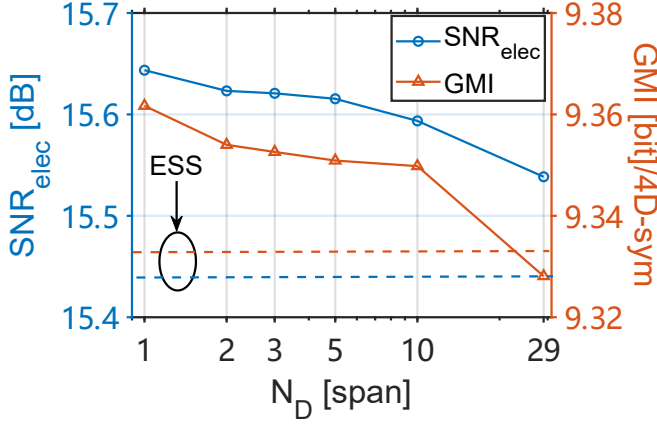


Fig. 10. Electrical SNR and GMI versus N_D for $D-E-ESS_1^4$, where each N_D value represents the following span indices used to compute D-EDI: $N_D = 1 \rightarrow [0 : 1 : 29]$; $2 \rightarrow [0, 1 : 2 : 29]$; $3 \rightarrow [0, 1, 2 : 3 : 29]$; $5 \rightarrow [0, 1, 4 : 5 : 29]$; $10 \rightarrow [0, 1, 9 : 10 : 29]$; $29 \rightarrow [0, 1, 29]$. We add the values for conventional ESS by horizontal dashed lines. Same system configuration as in Fig. 7. Gains are maintained even when we reduce the complexity by computing D-EDI over several spans.

of the selected sequences for multi-span transmissions.

Next, we explore the second reduced-complexity D-EDI computation method. Instead of computing EDI at the start of each span, we choose to compute it for fewer spans as explained in the caption of Fig. 10. The figure shows the performance variations in terms of SNR_{elec} and GMI versus N_D . We observe that, with increasing N_D , SNR experiences a gradual decline. Significantly, even with $N_D = 10$ (corresponding to EDI calculations every 800 km), the system still outperforms conventional ESS. In this case, computing D-EDI necessitates merely 5 evaluations, compared to 30 when $N_D = 1$ and resulting in a substantial reduction in computational complexity for D-EDI. This finding suggests that, for digital multi-band (DMB) transmissions over long-haul links, we can still achieve gains while using a reduced computational complexity metric for sequence selection.

To conclude this subsection, we highlight two key observations from the analyses in Fig. 9 and Fig. 10 for DMB transmissions over long-haul links: first, a sequence that performs well for D-EDI over fewer spans may not necessarily maintain its effectiveness over longer links. This observation underscores the complexity of sequence selection in optical communications. It is not sufficient to assess a sequence's suitability based solely on its performance at a single point, such as the beginning of a link or elsewhere, or at a part of the total distance. Second, identifying an optimal sequence does not require exhaustive analysis at the start of every span. Although dispersion-induced interference accumulates over longer distances, causing significant power variations and nonlinear phase fluctuations, our goal is to identify sequences that remain stable over distance. Since interference typically builds up over an extended period, involving the overlap of several symbols, it is practical to evaluate sequences at intervals spanning a few spans, rather than continuously or at every span.

C. The Impact of Block Length and Sequence Length Variations

Up to now, we have used a fixed block length of 108 for the comparison of our proposed schemes with state-of-the-art schemes in similar conditions. It is important to note that in the case of ESS, the block length has a significant impact on the performance (SNR and GMI). Decreasing the block length leads to increased nonlinear gain but also results in greater rate loss. Consequently, the optimal block length for ESS strikes a balance between maximizing nonlinear gain and minimizing rate loss. In Fig. 11, we plot the performance of ESS schemes for four different block lengths $l = \{60, 108, 200, 300\}$. The considered schemes are conventional ESS alongside D-E-ESS with 16 candidate sequences and D-E-ESS with 256 candidate sequences. With the increase of cascaded DMs and flipping bits, the number of candidate sequences can rapidly increase beyond 16 or 256. For example, when 4 serial DMs, each with 3 flipping bits, are concatenated, there are $2^{4 \times 3} = 4096$ candidate sequences. For these cases, we randomly select 16 or 256 sequences for selection. In Fig. 11, for each block length and each number of tested candidate sequences, we only show the best D-E-ESS performance found after testing various configurations of cascaded DMs and flipping bits. The main observations are:

- For the conventional ESS, as the block length increases, the SNR gradually decreases. Concurrently, the shortest block length of 60 provides a nonlinear gain that exceeds the relatively high rate loss, resulting in the maximum achievable GMI.
- For D-E-ESS, as the block length increases, the SNR slightly decreases. It has its maximum value at a block length of 60 and then levels off. At a block length of 60, the rate loss incurred by ESS itself, along with the additional rate loss from flipping bits, becomes too substantial for the achievable rate. Even though D-E-ESS exhibits a larger nonlinear gain, the final GMI falls short of what ESS offers.
- For longer block lengths, D-E-ESS consistently outperforms ESS due to its ability to maintain a significant nonlinear gain while mitigating excessive rate loss. Among these block lengths, D-E-ESS with a block length of 300 achieves the highest GMI.
- In particular, when the block length is equal to 300, D-E-ESS with 256 candidate sequences shows a 0.08-bit/4D GMI advantage over ESS with the same block length and a 0.04-bit/4D advantage over ESS with a block length of 60. D-E-ESS with 16 selections shows similar trends with slightly lower gains.

For a thorough analysis of the performance of D-E-ESS, we vary the sequence length under identical system configuration and report the performance in Fig. 12. We explore D-E-ESS configurations with three different block lengths and vary the number of cascaded DMs, resulting in multiple sequence lengths. For each sequence length, we report the optimal performance obtained by adjusting the number of flipping bits and by performing the selection among 16 (full lines) or 256 (dashed lines) candidate sequences. For ease of

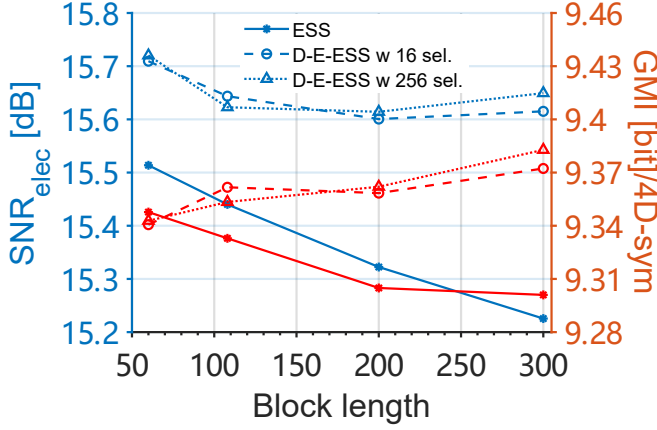


Fig. 11. Electrical SNR and GMI versus DM block length. We show the optimal performance for each block length by changing the number of flipping bits and the number of cascaded DMs. Same system configuration as in Fig. 7. D-E-ESS demonstrates superior performance over different block lengths.

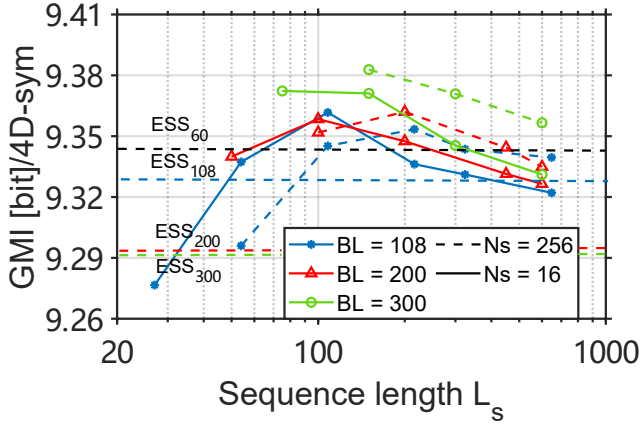


Fig. 12. GMI versus selected sequence length. We show the optimal performance versus different sequence lengths, for various block lengths, by changing the number of flipping bits and the number of cascaded DMs. Same system configuration as in Fig. 7. D-E-ESS demonstrates superior performance over different sequence lengths.

comparison, the performance of ESS with four block lengths is also depicted on the graph using horizontal dashed lines. When the block length is set to 300, D-E-ESS shows the best performance due to lower rate loss and comparable nonlinear behavior with respect to shorter block lengths. 256 selections tend to perform better for longer sequences because longer sequences necessitate cascading more DMs in series, hence providing more variability in the candidates for selection. With 256 selections, D-E-ESS can more effectively explore and utilize these possibilities. D-E-ESS significantly outperforms ESS across almost the entire range of tested sequence lengths for block lengths of 200 and 300. D-E-ESS with optimal sequence-length range (100 to 200 4D symbols) also surpasses the performance of ESS with block lengths of 60 and 108. The optimal sequence length for all four block lengths falls within the range of 100 to 200 4D symbols. We explain the observed behavior by the fact that overly long sequences capture more channel memory, yet they lead to coarser selections (at a

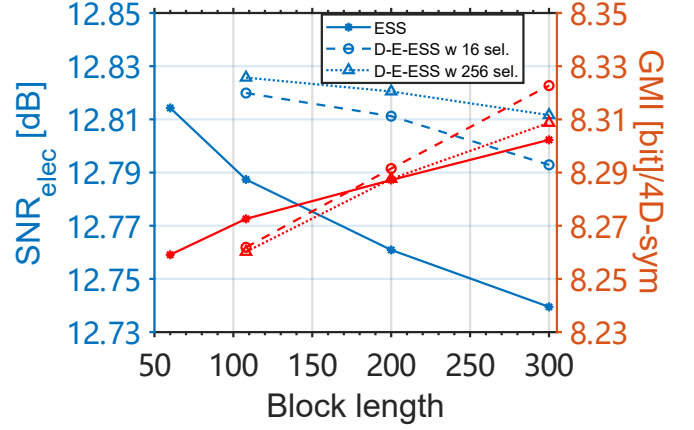


Fig. 13. Electrical SNR and GMI versus DM block length. We show the optimal point versus block length by changing the number of flipping bits and the number of cascaded DMs. Same system configuration as in Fig. 7, however with 5 WDM channels. D-E-ESS demonstrates superior performance in WDM transmission scenario.

fixed number of selections to limit the complexity). On the other hand, while very short sequences offer finer selections, they only capture a small fraction of the channel memory. Consequently, for the specific transmission scenario discussed in this article, the balance point between channel memory and selection precision lies within the range of 100 to 200 4D symbols.

D. WDM Transmission Performance

Finally, we maintain the same system configuration as before but extend it to a 5-channel WDM transmission. The combined net transmission rate for all five channels is 4.4 Tbits/s. In our earlier investigation, we observed poor performance for D-E-ESS with a block length of 60. Consequently, we assess the performance starting with a block length of 108. In Fig. 13, we see that, as the block length increases, the SNR_{elec} for ESS gradually decreases. However, the increase in GMI due to limited rate loss compensates for the reduction in nonlinear gain, yielding an optimal block length of 300 for ESS. Conversely, D-E-ESS better maintains nonlinear gains as the block length increases, and its rate loss continues to decrease. This results in D-E-ESS achieving the maximum GMI at a block length of 300. Particularly, with 16 selections, D-E-ESS with a block length of 300 outperforms ESS by 0.02 bits/4D-symbol, and it achieves a 0.06 bits/4D-symbol improvement compared to ESS with a block length of 60. Lastly, it is important to note that 256 selections, which require more flipping bits, lead to higher rate loss. The additional nonlinear gain does not fully compensate for the performance degradation caused by the increased rate loss, resulting in a lower GMI than with 16 selections. In a WDM configuration, the gains are lower than the ones observed in a single-channel system as in WDM, a high number of Cross-Phase Modulation components arise and our selection metric does not account for the energy dispersion of the neighboring channels.

VI. DISCUSSION AND CONCLUSION

We have proposed two reduced-complexity shaping schemes based on sequence selection and ESS. The first is based on a sign-independent metric (EDI), and the second is based on a sign-dependent metric (D-EDI). These new schemes achieved higher gains than state-of-the-art ESS schemes over short transmission distances. Noticably, D-E-ESS showed gains even for longer transmission distances and higher baud rates over single-channel and WDM systems even when CPR is used to reduce the impact of non-linear phase rotations. Concurrently, we showed that D-EDI can serve as a prediction metric of the generation of NLI because it showed a negative correlation with the measured performance of long-distance transmission systems. Moreover, D-E-ESS retained a robust performance at moderate complexity (lower number of digital dispersion operations to compute the metric) and outperformed conventional ESS across different block lengths. These results pave the way for further optimizations of shaping schemes for long-distance transmissions and confirm the necessity of using sign-dependent and channel-aware metrics for effectively mitigating nonlinear distortions using sequence selection. Nevertheless, these findings tell us that there is still room for improvement. The current probability shaping approach, based on sequence selection, revolves around three primary considerations:

- 1) Low-complexity candidate sequence generator: the method aims to maintain a low level of complexity for the generation of candidate sequences, allowing for a wider range of performance fluctuations. This enables a higher probability of selecting the optimal sequence and helps to improve the upper limit of sequence-selection performance.
- 2) Accurate and low-complexity measurement metric: precise measurements are employed to assess the non-linear performance of each candidate sequence. These measurements play a crucial role in determining which sequence is selected for transmission.
- 3) Matching of fixed sign bits and FEC encoding process in PCS schemes: another key consideration is to minimize complexity and reduce latency when matching fixed signs to FEC codewords. This optimization helps in improving the overall efficiency and applicability of the scheme.

In this paper, we improved the first two considerations. First, we used flipping bits to generate candidate sequences, instead of using LUTs and XOR-based bit scrambling methods as in [27]. This approach reduces the complexity of the scheme and avoids the additional memory requirements of LUTs. However, our D-EDI-based sequence selection exhibited almost the same performance improvement as the single-channel SSFM-based selection. This implies that we have reached the single-channel performance limit of sequence selection by flipping bits to generate sequences. To achieve further gains, we need to find better methods for the generation of sequences that exhibit larger possible performance variations, thus improving the upper limit of sequence-selection performance.

Second, we proposed a novel metric D-EDI which shows a negative correlation with the nonlinear performance of the

candidate sequence, and helps in achieving the same performance as the SSFM-based selection [27], however at a much lower complexity. Yet, for DMB-based transmissions in which the transmission rate per subcarrier is lower than single-carrier transmissions, the impact of channel memory is limited to a few symbols per span or even less than 1 symbol per span, hence only a few dozen symbols for all spans. Thus, the impact of channel memory can be accounted for by concatenating several DMs to minimize the mutual influence of adjacent selected sequences. As the transmission rates continue to increase, for both multi-carrier or single-carrier transmissions, the channel memory can spread over hundreds or thousands of symbols. At the same time, increasing the length of candidate sequences also increases the complexity of the scheme. Hence, modifications and optimizations of D-EDI to achieve excellent performance predictions under high-rate long-distance transmission while maintaining a reduced complexity is still an open question. Other improvements of the metric may address different dispersion management schemes or take into account inter-channel non-linear effects. In this work, we only considered long-haul dispersion-unmanaged systems where the NLI contributions from different spans can be considered independent and D-EDI gives a good performance prediction by summing up EDIs of the sequence at the start of each span.

Third, in this work, we used the multi-block FEC-independent structure proposed by [27], which fixes the signs of symbols and combines the fixed-signs sequence selection with FEC. However, the delay in this structure tends to be significant due to the encoding process involving multiple blocks, leading in this case to severe latency as the receiver should wait for the last block to be received before decoding. A lower-latency and lower-complexity matching method between fixed signs and FEC codewords is still to be discovered.

Ultimately, an extended goal involves conducting an in-depth analysis of the selected “good” sequences. By comprehensively understanding their properties, we aim to design simpler sequence generation solutions.

ACKNOWLEDGMENTS

This work was funded by Huawei Technologies France. We thank Yann Frignac for fruitful discussions.

REFERENCES

- [1] T. Pfau, S. Hoffmann, and R. Noé, “Hardware-efficient coherent digital receiver concept with feedforward carrier recovery for M -QAM constellations,” *Journal of Lightwave Technology*, vol. 27, no. 8, pp. 989–999, 2009.
- [2] K. Onohara, T. Sugihara, Y. Konishi, Y. Miyata, T. Inoue, S. Kametani, K. Sugihara, K. Kubo, H. Yoshida, and T. Mizuuchi, “Soft-Decision-Based Forward Error Correction for 100 Gb/s Transport Systems,” *IEEE Journal of Selected Topics in Quantum Electronics*, vol. 16, no. 5, pp. 1258–1267, 2010.
- [3] K. Kikuchi, “Fundamentals of Coherent Optical Fiber Communications,” *Journal of Lightwave Technology*, vol. 34, no. 1, pp. 157–179, 2016.
- [4] F. Frey, L. Molle, R. Emmerich, C. Schubert, J. K. Fischer, and R. F. H. Fischer, “Single-step Perturbation-based Nonlinearity Compensation of Intra- and Inter-Subcarrier Nonlinear Interference,” in *2017 European Conference on Optical Communication (ECOC)*, 2017, pp. 1–3.
- [5] F. R. Kschischang *et al.*, “Optimal nonuniform signaling for Gaussian channels,” *IEEE Transactions on Information Theory*, vol. 39, no. 3, pp. 913–929, 1993.

- [6] F. Buchali, F. Steiner, G. Böcherer, L. Schmalen, P. Schulte, and W. Idler, "Rate adaptation and reach increase by probabilistically shaped 64-qam: An experimental demonstration," *Journal of lightwave technology*, vol. 34, no. 7, pp. 1599–1609, 2015.
- [7] T. Fehenberger, A. Alvarado, G. Böcherer, and N. Hanik, "On probabilistic shaping of quadrature amplitude modulation for the nonlinear fiber channel," *Journal of Lightwave Technology*, vol. 34, no. 21, pp. 5063–5073, 2016.
- [8] Y. C. Gültekin, W. J. van Houtum, A. G. Koppelaar, F. M. Willems, J. Wim *et al.*, "Enumerative sphere shaping for wireless communications with short packets," *IEEE Transactions on Wireless Communications*, vol. 19, no. 2, pp. 1098–1112, 2019.
- [9] P. Schulte and G. Böcherer, "Constant composition distribution matching," *IEEE Transactions on Information Theory*, vol. 62, no. 1, pp. 430–434, 2015.
- [10] A. Alvarado, T. Fehenberger, B. Chen, and F. M. Willems, "Achievable information rates for fiber optics: Applications and computations," *Journal of Lightwave Technology*, vol. 36, no. 2, pp. 424–439, 2017.
- [11] T. Fehenberger, D. S. Millar, T. Koike-Akino, K. Kojima, K. Parsons, and H. Griesser, "Analysis of nonlinear fiber interactions for finite-length constant-composition sequences," *Journal of Lightwave Technology*, vol. 38, no. 2, pp. 457–465, 2019.
- [12] T. Fehenberger, H. Griesser, and J.-P. Elbers, "Mitigating fiber nonlinearities by short-length probabilistic shaping," in *Optical Fiber Communication Conference*. Optica Publishing Group, 2020, pp. Th11–2.
- [13] Y. C. Gültekin, O. Vassilieva, I. Kim, P. Palacharla, C. Okonkwo, and A. Alvarado, "On optimum enumerative sphere shaping blocklength at different symbol rates for the nonlinear fiber channel," in *2022 27th OptoElectronics and Communications Conference (OECC) and 2022 International Conference on Photonics in Switching and Computing (PSC)*. IEEE, 2022, pp. 1–3.
- [14] A. Amari, S. Goossens, Y. C. Gültekin, O. Vassilieva, I. Kim, T. Ikeuchi, C. M. Okonkwo, F. M. Willems, and A. Alvarado, "Introducing enumerative sphere shaping for optical communication systems with short blocklengths," *Journal of Lightwave Technology*, vol. 37, no. 23, pp. 5926–5936, 2019.
- [15] S. Civelli, E. Forestieri, and M. Secondini, "Interplay of probabilistic shaping and carrier phase recovery for nonlinearity mitigation," in *2020 European Conference on Optical Communications (ECOC)*. IEEE, 2020, pp. 1–4.
- [16] R. R. Borujeny and F. R. Kschischang, "Why constant-composition codes reduce nonlinear interference noise," *Journal of Lightwave Technology*, 2023.
- [17] Y. C. Gültekin, A. Alvarado, O. Vassilieva, I. Kim, P. Palacharla, C. M. Okonkwo, and F. M. Willems, "Kurtosis-limited sphere shaping for nonlinear interference noise reduction in optical channels," *Journal of Lightwave Technology*, vol. 40, no. 1, pp. 101–112, 2021.
- [18] A. Carena, G. Bosco, V. Curri, Y. Jiang, P. Poggiolini, and F. Forghieri, "Egn model of non-linear fiber propagation," *Optics express*, vol. 22, no. 13, pp. 16 335–16 362, 2014.
- [19] Y. C. Gültekin, A. Alvarado, O. Vassilieva, I. Kim, P. Palacharla, C. M. Okonkwo, and F. M. J. Willems, "Mitigating nonlinear interference by limiting energy variations in sphere shaping," in *2022 Optical Fiber Communications Conference and Exhibition (OFC)*, 2022, pp. 1–3.
- [20] J. Liu, E. Awwad, and Y. Jaouen, "Multi-dimensional Energy Limitation in Sphere Shaping for Nonlinear Interference Noise Mitigation," in *Asia Communications and Photonics Conference*. IEEE, 2023.
- [21] K. Wu, G. Liga, A. Sheikh, F. M. Willems, and A. Alvarado, "Temporal energy analysis of symbol sequences for fiber nonlinear interference modelling via energy dispersion index," *Journal of Lightwave Technology*, vol. 39, no. 18, pp. 5766–5782, 2021.
- [22] K. Wu, G. Liga, A. Sheikh, Y. C. Gültekin, F. M. Willems, and A. Alvarado, "List-encoding CCDF: A nonlinearity-tolerant shaper aided by energy dispersion index," *Journal of Lightwave Technology*, vol. 40, no. 4, pp. 1064–1071, 2022.
- [23] M. T. Askari, L. Lampe, and J. Mitra, "Probabilistic amplitude shaping and nonlinearity tolerance: Analysis and sequence selection method," *Journal of Lightwave Technology*, 2023.
- [24] Askari, Mohammad Taha and Lampe, Lutz and Mitra, Jeebak, "Non-linearity tolerant shaping with sequence selection," in *2022 European Conference on Optical Communication (ECOC)*. IEEE, 2022, pp. 1–4.
- [25] S. Civelli, E. Forestieri, A. Lotsmanov, D. Razdoburdin, and M. Secondini, "A sequence selection bound for the capacity of the nonlinear fiber channel," in *2021 European Conference on Optical Communication (ECOC)*. IEEE, 2021, pp. 1–4.
- [26] M. Secondini, S. Civelli, E. Forestieri, and L. Z. Khan, "New lower bounds on the capacity of optical fiber channels via optimized shaping and detection," *Journal of Lightwave Technology*, vol. 40, no. 10, pp. 3197–3209, 2022.
- [27] S. Civelli, E. Forestieri, and M. Secondini, "Sequence-selection-based constellation shaping for nonlinear channels," *Journal of Lightwave Technology*, 2023.
- [28] P. Skvortcov, I. Phillips, W. Forysiak, T. Koike-Akino, K. Kojima, K. Parsons, and D. S. Millar, "Huffman-coded sphere shaping for extended-reach single-span links," *IEEE Journal of Selected Topics in Quantum Electronics*, vol. 27, no. 3, pp. 1–15, 2021.
- [29] G. P. Agrawal, "Nonlinear fiber optics," in *Nonlinear Science at the Dawn of the 21st Century*. Springer, 2000, pp. 195–211.
- [30] T. Fehenberger, M. P. Yankov, L. Barletta, and N. Hanik, "Compensation of xpm interference by blind tracking of the nonlinear phase in wdm systems with qam input," in *2015 European Conference on Optical Communication (ECOC)*. IEEE, 2015, pp. 1–3.
- [31] G. Böcherer, "Probabilistic signal shaping for bit-metric decoding," in *2014 IEEE International Symposium on Information Theory*, 2014, pp. 431–435.
- [32] J. Cho, X. Chen, G. Raybon, D. Che, E. Burrows, S. Olsson, and R. Tkach, "Shaping lightwaves in time and frequency for optical fiber communication," *Nature communications*, vol. 13, no. 1, p. 785, 2022.
- [33] A. Lorences-Riesgo, M. S. Neves, C. S. Martins, S. Mumtaz, P. A. Loureiro, Y. Frignac, P. P. Monteiro, G. Charlet, F. P. Guiomar, and S. Dris, "Improving nonlinearity tolerance of pcs-qam digital multi-carrier systems through symbol rate optimization," in *European Conference and Exhibition on Optical Communication*. Optica Publishing Group, 2022, pp. We1C–3.
- [34] P. Poggiolini, G. Bosco, A. Carena, V. Curri, Y. Jiang, and F. Forghieri, "The gn-model of fiber non-linear propagation and its applications," *Journal of lightwave technology*, vol. 32, no. 4, pp. 694–721, 2013.